| | |
|---|---|
| Title | Characterization of attosecond XUV pulses utilizing a broadband UV-VUV pumping |
| Author(s) | Chen, Jun; Itakura, Ryuji; Nakajima, Takashi |
| Citation | Optics Express (2010), 18(3): 2020-2035 |
| Issue Date | 2010 |
| URL | http://hdl.handle.net/2433/108362 |
| Right | (c) 2010 Optical Society of America |
| Type | Journal Article |
| Textversion | author |

# Characterization of attosecond XUV pulses utilizing a broadband UV∼VUV pumping

**Jun Chen,[1†] Ryuji Itakura, [2] and Takashi Nakajima [1*]**

[1] *Institute of Advanced Energy, Kyoto University, Gokasho, Uji, Kyoto 611-0011, Japan*

[2] *Kansai Photon Science Institute, Japan Atomic Energy Agency, 8-1-7 Umemidai, Kizugawa, Kyoto 619-0215, Japan*

[*] *t-nakajima@iae.kyoto-u.ac.jp*

**Abstract:**
We propose a simple scheme to characterize attosecond extreme ultraviolet (XUV) pulses. A broadband ultraviolet (UV) ∼ vacuum ultraviolet (VUV) pump pulse creates a coherent superposition of atomic bound states, from which photoionization takes place by the time-delayed attosecond XUV probe pulse. Information on the spectral phase of the XUV pulse can be extracted from the phase offset of the interference beating in the photoelectron spectra using a standard SPIDER (spectral phase interferometry for direct electric-field reconstruction) algorithm. We further discuss the influence of the chirp and polychromaticity of the pump pulse, and show that they do not spoil the reconstruction process. Since our scheme is applicable for various simple atoms such as H, He, and Cs, etc., and capable of characterizing attosecond XUV pulses with a pulse duration of a few hundred attoseconds or even less, it can be an alternative technique to characterize attosecond XUV pulses. Specific numerical examples are presented for the H atom utilizing the $2p$ and $3p$ states.



**OCIS codes:** (320.7100) Ultrafast optics: Ultrafast measurements; (320.7110) Ultrafast optics: Ultrafast nonlinear optics.

## References and links

1. F. Krausz and M. Ivanov,"Attosecond physics," Rev. Mod. Phys. **81**, 163-234(2009).
2. Pierre Agostini and Louis F DiMauro, "The physics of attosecond light pulses," Rep. Prog. Phys. **67**, 813-855(2004).
3. R. Trebino, K. W. Delong, D. N. Fittinghoff, J. N. Sweetser, M. A. Krumbügel, B. A. Richman and D. J. Kane, "Measuring ultrashort laser pulses in the time-frequency domain using frequency-resolved optical gating," Rev. Sci. Instrum. **68**, 3277-3295 (1997).
4. C. Iaconis and I. A. Walmsley, "Spectral phase interferometry for direct electric-field reconstruction of ultrashort optical pulses," Opt. Lett. **23**, 792-794(1998).
5. C. Iaconis and I. A. Walmsley, "Self-Referencing Spectral Interferometry for Measuring Ultrashort Optical Pulses," IEEE J. Quantum Electron. **35**, 501-509(1999).
6. J. Norin, J. Mauritsson, A. Johansson, M. K. Raarup, S. Buil, A. Persson, O. Dühr, M. B. Gaarde, K. J. Schafer, U. Keller, C.-G. Wahlström, and A. LHuillier, "Time-Frequency Characterization of Femtosecond Extreme Ultraviolet Pulses," Phys. Rev. Lett. **88**, 193901(2002).
7. T. Sekikawa, T. Katsura, S. Miura, and S. Watanabe, "Measurement of the Intensity-Dependent Atomic Dipole Phase of a High Harmonic by Frequency-Resolved Optical Gating," Phys. Rev. Lett. **88**, 193902(2002).

8. Y. Mairesse and F. Quéré, "Frequency-resolved optical gating for complete reconstruction of attosecond bursts," Phys. Rev. A **71**, 011401(R)(2005).
9. F. Quéré, Y. Mairesse and J. Itatani, "Temporal characterization of attosecond XUV fields," J. Mod. Opt., **52**, 339-360(2005).
10. E. Cormier, I. A. Walmsley, E. M. Kosik, A. S. Wyatt, L. Corner, and L. F. DiMauro, "Self-Referencing, Spectrally, or Spatially Encoded Spectral Interferometry for the Complete Characterization of Attosecond Electromagnetic Pulses," Phys. Rev. Lett. **94**, 033905(2005).
11. E. Cormier, L. Corner, E. M. Kosik, I. A. Walmsley, and A. S. Wyatt, "Spectral Phase Interferometry for Complete Reconstruction of Attosecond Pulses," Laser Phys., **15**, 1-7(2005).
12. P. M. Paul, E. S. Toma, P. Breger, G. Mullot, F. Augé, Ph. Balcou, H. G. Muller, P. Agostini, "Observation of a Train of Attosecond Pulses from High Harmonic Generation," Science **292**, 1689-1692(2001).
13. H. G. Muller, "Reconstruction of attosecond harmonic beating by interference of two-photon transitions," Appl. Phys. B **74**, S17-S21(2002).
14. Y. Nabekawa, T. Shimizu, T. Okino, K. Furusawa, H. Hasegawa, K. Yamanouchi, and K. Midorikawa, "Interferometric autocorrelation of an attosecond pulse train in the single-cycle regime," Phys. Rev. Lett. **97**, 153904 (2006).
15. R. Itakura, "Spectral phase measurement of attosecond pulses using the quantum beat between the $P_{1/2}$ and $P_{3/2}$ levels of alkali-metal atoms," Phys. Rev. A **76**, 033810(2007).
16. J. Chen and T. Nakajima, "Characterization of Attosecond XUV Pulses from Photoelectron Spectra of Atoms," Laser Phys. **19**, 1586-1590(2009).
17. T. Sekikawa, T. Okamoto, E. Haraguchi, M. Yamashita, and T. Nakajima, "Two-photon resonant excitation of a doubly excited state in He atoms by high-harmonic pulses," Opt. Express **16**, 21922-21929 (2008).
18. T. Nakajima, "Possibility of direct determination of the quantum phase of continua utilizing the phase of lasers," Phys. Rev. A **61**, 041403(R)(2000).
19. C. Dorrer and I. A. Walmsley, "Accuracy criterion for ultrashort pulse characterization techniques: application to spectral phase interferometry for direct electric field reconstruction," J. Opt. Soc. Am. B **19**, 1019-1029 (2002).
20. M. E. Anderson, L. E. E. de Araujo, E.M.Kosik and I.A.Walmsley, "The effects of noise on ultrashort-optical-pulse measurement using SPIDER", Appl. Phys. B, **70**[Suppl.], S85-S93(2000).
21. N. Rahman "The degenerate two-level system and high-order harmonic generation," Chem. Phys. Lett. **270**, 189-192 (1997).
22. Y. Kobayashi, T. Ohno, T. Sekikawa, Y. Nabekawa, S.Watanabe, "Pulse width measurement of high-order harmonics by autocorrelation," Appl. Phys. B **70**, 389-394 (2000).
23. S. Zamith, J. Degert, S. Stock, B. de Beauvoir, V. Blanchet, M. A. Bouchene and B. Girard,"Observation of Coherent Transients in Ultrashort Chirped Excitation of an Undamped Two-Level System," Phys. Rev. Lett. **87**, 033001(2001).
24. T. Nakajima, "Effects of the carrier-envelope phase on atomic ionization by the pulse train in the multiphoton ionization regime, " Phys. Rev. A **79**, 043414 (2009).

† Current address: College of Optical and Electronic Technology, China Jiliang University, Hangzhou 310018, China

## 1. Introduction

The generation of attosecond pulses in the XUV range offers us a novel tool to investigate/control ultrafast electronic processes in the target [1]. Obviously establishing accurate metrologies for such pulses plays a crucial role in the development of attosecond science [2]. However, a complete characterization of attosecond XUV pulses is a challenging task because of the lack of an appropriate nonlinear medium and an insufficient intensity to induce any relevant nonlinear processes. Therefore standard ultrashort pulse measurement techniques such as FROG (frequency-resolved optical gating) [3] and SPIDER [4, 5] can not be directly applied to characterize attosecond XUV pulses.

By using two-photon ionization as a nonlinear process [6, 7] or by applying a dressing laser field as a phase-modulation gate [8, 9], FROG can be extended to characterize XUV femtosecond/attosecond pulses. Similarly several schemes have been considered to extend SPIDER into the XUV range. Generally speaking, they can be classified into two kinds. The first kind is based on the spectral shear interferometry in which frequency-sheared replicas of the attosecond XUV pulse are generated by manipulating the driving laser pulse [10, 11]. The second kind utilizes photoionization induced by the attosecond XUV pulse, where information of the XUV pulse is transferred to the photoelectron spectrum [12, 13, 14]. Although the former methods

are robust, preparation for the frequency-sheared replicas of the attosecond XUV pulse remains a major difficulty for experimental realization. The latter methods are more commonly used in attosecond metrology. Clearly such methods may be considered as photoelectron variants of optical SPIDER. Indeed it was recently shown that the combined use of a near-infrared femtosecond pulse and a time-delayed XUV pulse results in a quantum beat in the photoelectron spectra of Cs atoms, from which the XUV pulse can be reconstructed using the standard SPIDER algorithm (Cs-SPIDER) [15]. Unfortunately, the temporal period of the beat is at best in the order of tens of fs if one utilizes an atomic fine structure doublet, indicating that the Cs-SPIDER may not be a good scheme to characterize attosecond XUV pulses. That is, the energy shear induced in photoelectrons through the coherent preparation of a Cs fine structure doublet by the pump pulse is too small to characterize attosecond XUV pulses with an enormous bandwidth ($>$a few eV) [16]. Recall that the amount of the frequency shear is quite important for the case of optical SPIDER, and the similar is true for the Cs-SPIDER and its variant studied here.

The purpose of this paper is to propose a new scheme similar to the Cs-SPIDER and show that our scheme is particularly suitable to characterize attosecond XUV pulses. For that purpose we employ a broadband UV$\sim$VUV pump pulse to create a coherent superposition of electronically excited states (with *different* principal quantum numbers) instead of a fine structure doublet (with the *same* principal quantum number), resulting in more than one order of magnitude larger energy shear. There are a few other nice features for the present scheme. The first one is that the present scheme as well as the Cs-SPIDER can characterize both pulse train and isolated pulse. The second one is that, as we will explain later on, the (linear or nonlinear) chirp and the temporal form (isolated pulse or pulse train) of the pump pulse does not influence the reconstruction process of the XUV probe pulse at all as long as they remain the same throughout the SPIDER measurement. The third one is that we can employ any simple (one-electron) atoms such as H and Cs, and also some of the more complex (two-electron) but well-studied atoms such as He for target atoms, for which wavefunctions are accurately known. The use of accurately known atoms enables us to carry out the field reconstruction without any well-established but still big approximation such as strong field approximation employed, for instance, in FROG-CRAB [8, 9]. The major drawback of our scheme is that the photoelectron signal will not be as strong as that of FROG-CRAB due to the use of one-photon *resonant* two-photon ionization by the UV$\sim$VUV pump and XUV probe pulses in the perturbation regime. But we believe it will not a big problem in these days, since even *nonresonant* two-photon above-threshold ionization of He by XUV (30 eV) photons has been experimentally observed in recent experiments [17] with a good agreement with a theory. After the derivation of all necessary equations we perform some analysis from the few different aspects before presenting numerical results for the H atom as an example. Both of our analysis and numerical results demonstrate the capability of our scheme for the reconstruction of attosecond XUV pulses.

## 2. Photoelectron SPIDER with a UV$\sim$VUV pumping

Although our scheme works well for any simple (one-electron) atoms such as H, Rb, and Cs, and some of the more complicated atoms such as He, we specifically focus on the H atom in this paper for maximum clarity. The level scheme we consider is shown in Fig. 1. H atoms in the ground state 1$s$, labeled as $|0\rangle$, are coherently excited to states 2$p$ and 3$p$, labeled as $|1\rangle$ and $|2\rangle$, respectively, by the broadband VUV pump pulse with linear polarization whose polarization vector is parallel to the quantization axis. Naturally if we use other atoms such as Cs, $|1\rangle$ and $|2\rangle$ may be, for instance, 6$p$ and 7$p$, or 7$p$ and 8$p$, etc., and the pump pulse is in the UV range. Note that the fine structure may be safely neglected in our case since the associated energy splitting results in the very slow modulation in the photoelectron signal when plotted

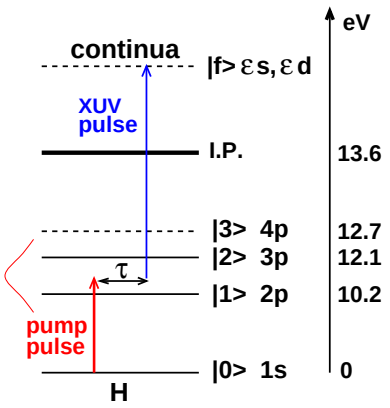


Fig. 1. Level scheme of hydrogen atom. The broadband pump (VUV) pulse with an appropriate central photon energy creates a coherent superposition in states $|1\rangle$ and $|2\rangle$, from which photoionization takes place by the time-delayed attosecond probe (XUV) pulse. If the pump pulse is very broad, it may also excite the next neighboring state, $|3\rangle$. The possible ionization continua, $|f\rangle$, are $\varepsilon s$ and $\varepsilon d$ where $\varepsilon$ represents the energy of photoelectrons.

as a function of delay time between the pump and probe pulses. Which atoms and states are more appropriate for the measurement depends on the available wavelength of the pump pulse as well as the bandwidths of the pump and probe pulses. We note that the pump pulse does not have to be transform-limited. It may have some arbitrary (linear or nonlinear) chirp. The detailed discussion for the chirp of the pump pulse is postponed until we come to Sec. 4. For simplicity we assume, for a moment, that both pump and probe pulses are isolated pulses. But later in this paper we will lift this restriction and argue that either or both of pump and probe pulses can be a pulse train(s). The wavefunction of the excited states, $|\psi_{\rm coh}(t)\rangle$, can be written as

$$|\psi_{\rm coh}(t)\rangle = \sum_k C_k \exp\left[-i\omega_k t\right]|k\rangle \quad (k=1,2), \tag{1}$$

where $C_k$ and $\omega_k$ $(k=1,2)$ are the complex probability amplitude of state $|k\rangle$ and its frequency, respectively. After a time delay, $\tau$, the attosecond XUV pulse induces photoionization into the continua represented by $\varepsilon s$ and $\varepsilon d$ where $\varepsilon$ stands for the energy of photoelectrons. For a given kinetic energy $\varepsilon$ and orbital angular quantum number $l$, the continuum state of the outgoing photoelectron is expressed as [18]

$$|f(\varepsilon,l,\mathbf{\Omega})\rangle = \sum_{m_l} i^l \exp\left[-i\sigma_l(\varepsilon)\right] Y^*_{lm_l}(\mathbf{\Omega})|R_{\varepsilon l}\rangle|lm_l\rangle, \tag{2}$$

in which $\sigma_l(\varepsilon)$ is a sum of the Coulomb phase shift given by $\sigma_l^C(\varepsilon) = \arg[\Gamma(l+1-i/\sqrt{\varepsilon})] - l\pi/2$ with $\varepsilon$ being the photoelectron energy in Rydberg units and the non-Coulomb (scattering) phase shift, $\sigma_l^{NC}(\varepsilon)$, for the photoelectron with an orbital quantum number $l$, i.e., $\sigma_l(\varepsilon) = \sigma_l^C(\varepsilon) + \sigma_l^{NC}(\varepsilon)$. Of course $\sigma_l^{NC}(\varepsilon) = 0$ for the H atom. $Y_{lm_l}(\mathbf{\Omega})$ is the spherical harmonics and represents an angular distribution of photoelectrons into the direction given by $\mathbf{\Omega} = (\Theta,\Phi)$ for the orbital quantum number $l$ and its projection onto the quantization axis, $m_l$. $|R_{\varepsilon l}\rangle$ is a radial wavefunction of the continuum. When there is no temporal overlap between the pump and probe pulses, the photoionization amplitude into the continuum state, $|f(\varepsilon,l,\mathbf{\Omega})\rangle$, reads

$$M_f(\varepsilon,l,\mathbf{\Omega},\tau) = \langle f(\varepsilon,l,\mathbf{\Omega})|\mathbf{E}^{\rm xuv}(\omega)\cdot\mathbf{r}|\psi_{\rm coh}(\tau)\rangle\,, \tag{3}$$

where $\mathbf{E}^{\mathrm{xuv}}(\omega)$ is the spectral field amplitude of the attosecond XUV pulse to be characterized, i.e.,

$$\mathbf{E}^{\mathrm{xuv}}(\omega) = \sqrt{I^{\mathrm{xuv}}(\omega)}\exp\left[-i\phi^{\mathrm{xuv}}(\omega)\right], \tag{4}$$

with $I^{\mathrm{xuv}}(\omega)$ and $\phi^{\mathrm{xuv}}(\omega)$ being the spectral intensity and spectral phase, respectively. Given the photoelectron energy, $\varepsilon$, detection angle, $\Theta$, and time delay, $\tau$, we can calculate the photoelectron angular distribution, $S(\varepsilon,\Theta,\tau)$, through the relation of

$$\begin{aligned} S(\varepsilon,\Theta,\tau) &= \frac{dP(\varepsilon,\mathbf{\Omega},\tau)}{d\mathbf{\Omega}} \\ &= \sum_{l}\left|M_f(\varepsilon,l,\mathbf{\Omega},\tau)\right|^2 \\ &= \sum_{l,k,k'} C_k^* C_{k'} M_{fk}^*(\varepsilon,l,\Theta) M_{fk'}(\varepsilon,l,\Theta)\exp[i(\omega_{k'}-\omega_k)\tau] \\ &\equiv S_{11}(\varepsilon,\Theta,\tau)+S_{22}(\varepsilon,\Theta,\tau)+S_{21}(\varepsilon,\Theta,\tau), \end{aligned} \tag{5}$$

where $P(\varepsilon,\mathbf{\Omega},\tau)$ is the photoelectron signal, and $M_{fk}(\varepsilon,l,\Theta)$ is the monochromatic photoionization probability amplitude from $|k\rangle$ to $|f(\varepsilon,l,\mathbf{\Omega})\rangle$. $S_{kk}(\varepsilon,\Theta,\tau)$ $(k=1,2)$ represents the photoelectron angular distribution from state $|k\rangle$. Since photoionization takes place from the coherently excited state given by Eq. (1), a cross term, $S_{21}(\varepsilon,\Theta,\tau)$, appears in Eq. (5). Clearly the cross term oscillates as a function of delay time at a frequency $\omega_{k'k}=|\omega_{k'}-\omega_k|$, which is nothing but a quantum beat.

For simplicity we assume that the attosecond XUV pulse is also linearly polarized with a polarization vector parallel to that of the pump pulse. Then the final continuum states can have *s* and *d* symmetries as shown in Fig. 1. Since these continua are associated with the spherical harmonics, $Y_{00}$ and $Y_{20}$ in Eq. (2), respectively, which have different angular distributions, we can collect the photoelectron signal from the *s* wave only if we set the detection angle at $\Theta_0=\cos^{-1}(1/\sqrt{3})$ or $\pi-\cos^{-1}(1/\sqrt{3})$ (magic angle). Setting the detection angle at $\Theta_0$, we can simplify Eq. (5). The most important term is the cross term, and it can be recast into the simplified form of

$$S_{21}(\varepsilon,\Theta_0,\tau) \propto \mathscr{R}_{s1}\mathscr{R}_{s2}|C_1^*C_2|\sqrt{I^{\mathrm{xuv}}(\omega)I^{\mathrm{xuv}}(\omega-\omega_{21})}\cos\left[\omega_{21}\tau+\phi_c-\Delta\phi_{21}^{\mathrm{xuv}}(\omega)\right], \tag{6}$$

in which $\mathscr{R}_{sk}$ $(k=1,2)$ is the radial component of the bound-free dipole moment between $|k\rangle$ and $|\varepsilon s\rangle$, and $\phi_c=\arg[C_1^*C_2]$. In Eq. (6), $\omega$ represents a frequency component of the attosecond XUV pulse, and it is connected to the photoelectron energy, $\varepsilon$, through the relation of

$$\omega = (\varepsilon+E_{\mathrm{IP}})/\hbar-\omega_1, \tag{7}$$

with $E_{\mathrm{IP}}=13.6$ eV being the ionization potential of H, and the phase offset, $\Delta\phi_{21}^{\mathrm{xuv}}(\omega)$, physically represents a spectral phase difference of the attosecond XUV pulse with a frequency interval of $\omega_{21}=\omega_2-\omega_1$, i.e.,

$$\Delta\phi_{21}^{\mathrm{xuv}}(\omega) = \phi^{\mathrm{xuv}}(\omega-\omega_{21})-\phi^{\mathrm{xuv}}(\omega). \tag{8}$$

Once the spectral phase difference, $\Delta\phi_{21}^{\mathrm{xuv}}(\omega)$, has been measured at a discrete set of frequencies $\{\omega_i,\omega_i\in[\omega_{\min},\omega_{\max}]\}$ where $\omega_{\min}$ and $\omega_{\max}$ represents the minimum and maximum frequency having nonzero spectral intensity, respectively, the spectral phase of the XUV pulse, $\phi^{\mathrm{xuv}}(\omega)$, can be obtained with the standard algorithm for the optical SPIDER [15, 19], i.e.,

$$\phi^{\mathrm{xuv}}(\omega) \doteq \frac{1}{-\omega_{21}} \sum_{\omega_{\min}}^{\omega-\omega_{21}/2} \Delta\phi_{21}^{\mathrm{xuv}}(\omega_i)\Delta\omega_i. \tag{9}$$

In the above equation $\Delta\omega_i$ is determined by the frequency resolution of the measurement. Together with the information on the spectral intensity, $I^{\mathrm{xuv}}(\omega)$, which can be obtained from a separate optical measurement, we have now sufficient information to reconstruct the temporal electric field of the attosecond XUV pulse through the Fourier transform of the spectral electric field.

In the above discussion we have implicitly assumed that the acceptable angle of a detector set at the magic angle is infinitely small. In reality, however, any photoelectron detector has a finite width for the detection angle. In order to take into account the finite width for the detection angle around the magic angle, $\Theta_0 \pm \delta$, where $\delta$ is the maximum deviation from $\Theta_0$, we must derive a general expression for the beat signal detected at an arbitrary angle, $\Theta$. It reads

$$S_{21}(\varepsilon,\Theta,\tau) \propto S_{21}(\varepsilon,\Theta_0,\tau) + B(\varepsilon,\tau)(3\cos^2\Theta - 1)^2 + A(\varepsilon,\tau)(3\cos^2\Theta - 1), \tag{10}$$

where

$$B(\varepsilon,\tau) = \frac{5}{4}\mathscr{R}_{d1}\mathscr{R}_{d2}|C_1^* C_2|\sqrt{I^{\mathrm{xuv}}(\omega)I^{\mathrm{xuv}}(\omega-\omega_{21})}\cos\left[\omega_{21}\tau + \phi_c - \Delta\phi_{21}^{\mathrm{xuv}}(\omega)\right], \tag{11}$$

and

$$\begin{aligned} A(\varepsilon,\tau) = &-\frac{\sqrt{5}}{2}|C_1^* C_2|\sqrt{I^{\mathrm{xuv}}(\omega)I^{\mathrm{xuv}}(\omega-\omega_{21})} \\ &\times \left\{(\mathscr{R}_{s1}\mathscr{R}_{d2} + \mathscr{R}_{d1}\mathscr{R}_{s2})\cos\left[\sigma_d(\varepsilon) - \sigma_s(\varepsilon)\right]\cos\left[\omega_{21}\tau + \phi_c - \Delta\phi_{21}^{\mathrm{xuv}}(\omega)\right]\right. \\ &\left. - \ (\mathscr{R}_{s1}\mathscr{R}_{d2} - \mathscr{R}_{d1}\mathscr{R}_{s2})\sin\left[\sigma_d(\varepsilon) - \sigma_s(\varepsilon)\right]\sin\left[\omega_{21}\tau + \phi_c - \Delta\phi_{21}^{\mathrm{xuv}}(\omega)\right]\right\}. \end{aligned} \tag{12}$$

In the above equations $\mathscr{R}_{dk}$ $(k = 1,2)$ is the radial component of the bound-free dipole moment between $|k\rangle$ and $|\varepsilon d\rangle$. Note that we now have a contribution of the $d$ wave in addition to the $s$ wave. From Eqs. (11) and (12), we can see that the beat pattern of $B(\varepsilon,\tau)$ is exactly the same with that of $S_{21}(\varepsilon,\Theta_0,\tau)$ [see Eq. (6)], while that of $A(\varepsilon,\tau)$ is different. The beat pattern of $A(\varepsilon,\tau)$ is related to the values of the phase shifts, $\sigma_s(\varepsilon)$ and $\sigma_d(\varepsilon)$, and the radial components of the bound-free dipole moments, $\mathscr{R}_{sk}$ and $\mathscr{R}_{dk}$ $(k = 1,2)$, all of which are differently behaving functions of photoelectron energy, $\varepsilon$. Because the spectral phase difference, $\Delta\phi_{21}^{\mathrm{xuv}}(\omega)$, which is the main physical quantity of our interest, is also a function of $\varepsilon$, neglecting the $A(\varepsilon,\tau)$ term would bring an error in the determination of the spectral phase if the width of the detection angle is finite.

Once the beat signal at an arbitrary angle $\Theta$ has been obtained, we can perform the solid angle integration of Eq. (10) for the beat signal at the detector with a finite width for the detection angle, i.e., $\Theta_0 - \delta < \Theta < \Theta_0 + \delta$. The beat signal at the detector, $P_{21}(\varepsilon,\tau)$, can now be evaluated through the following integration:

$$\begin{aligned} P_{21}(\varepsilon,\tau) &= \int_\Omega S_{21}(\varepsilon,\Theta,\tau)\, d\Omega \\ &= 2\delta \int_{\Theta_0-\delta}^{\Theta_0+\delta} S_{21}(\varepsilon,\Theta,\tau)\sin\Theta\, d\Theta \end{aligned}$$

$$\propto \mathscr{R}_{s1}\mathscr{R}_{s2}|C_1^*C_2|\sqrt{I^{\rm xuv}(\omega)I^{\rm xuv}(\omega-\omega_{21})}$$
$$\times\cos\left[\omega_{21}\tau+\phi_c-\left(\Delta\phi_{21}^{\rm xuv}(\omega)+\Delta\tilde{\beta}(\delta,\omega)\right)\right], \tag{13}$$

where $\Delta\tilde{\beta}(\delta,\omega)$ is an additional spectral phase difference originated from the finite width for the detection angle. Therefore, the spectral phase of the XUV pulse reconstructed from the beat signal at the detector is

$$\phi_{\rm dector}^{\rm xuv}(\delta,\omega)=\phi^{\rm xuv}(\omega)+\tilde{\beta}(\delta,\omega), \tag{14}$$

where

$$\tilde{\beta}(\delta,\omega)\doteq\frac{1}{-\omega_{21}}\sum_{\omega_{\rm min}}^{\omega-\omega_{21}/2}\Delta\tilde{\beta}(\delta,\omega_i)\Delta\omega_i. \tag{15}$$

is a spectral phase error.

In order to quantitate the spectral phase error $\tilde{\beta}(\delta,\omega)$ due to the finite width for the detection angle, i.e., $\Theta_0-\delta<\Theta<\Theta_0+\delta$, we numerically reconstruct the spectral phase of the attosecond XUV pulse using Eqs. (13)-(15). Note that the spectral phase error retrieved from the spectral phase difference error, $\Delta\tilde{\beta}(\delta,\omega)$, is a *relative* quantity. Therefore, by recalling Eq. (10), we realize that the reference point to evaluate the spectral phase error can be chosen at any energy point to retrieve the spectral phase distribution as functions of photoelectron energy and time. Specifically we choose the reference point at the central photon energy of the XUV pulse to be characterized, which is assumed to be 30 eV. In Fig. 2 we plot the spectral phase error as a function of photon energy for the three different angle widths, $\delta=5^{\rm o}$, $10^{\rm o}$, and $20^{\rm o}$. We can see that the spectral phase error arising from the finite width for the detection angle is rather small even for $\delta=20^{\rm o}$. Based on this result, from now on we will neglect the influence of the finite width for the detection angle.

In this section we have shown the scheme for the reconstruction of the temporal field of attosecond XUV pulses. Compared with the one described in Ref. [15] utilizing the fine structure doublet of Cs, the present scheme benefits from the much larger energy shear arising from the much larger energy separation between the two different electronic states, which enables us to

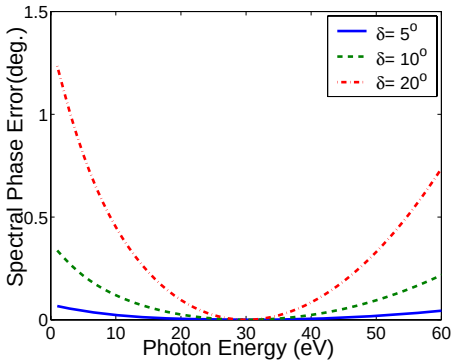


Fig. 2. Representative results of the spectral phase error $[-\tilde{\beta}(\delta,\omega)]$ contained in the reconstructed spectral phase distribution, $[-\phi_{\rm detector}^{\rm xuv}(\omega)]$, as a function of probe photon energy. The solid blue, dashed green, and dot-dashed red curves represent results for the three different angle widths of $\delta=5^{\rm o}$, $10^{\rm o}$, and $20^{\rm o}$, respectively.

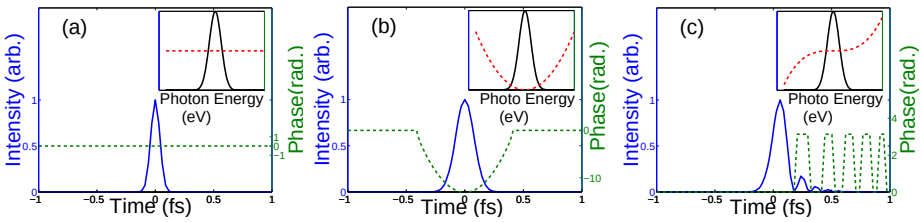


Fig. 3. Probe pulse shapes employed for the error estimation of the reconstructed pulses. The temporal intensity (blue solid line) and temporal phase (green dashed line) are shown for the (a) transform-limited, (b) linearly chirped, and (c) quadratically chirped pulses. In each graph the inset shows the corresponding pulse spectrum (black solid line) and spectral phase (red dashed line). All pulses are assumed to have the identical Gaussian spectrum with a FWHM of 20 eV and the central photon energy of 30 eV.

characterize attosecond XUV pulses with much better accuracy through the much faster quantum beat in the photoelectron signals. The reason can be explained using Eq. (8): It shows that the spectral phase of the attosecond XUV pulse to be characterized is sampled by the quantum beat at a frequency interval of $\omega_{21}$. The fine structure doublet in Ref. [15] can provide a small energy shear (0.069 eV) through the quantum beat. To reconstruct attosecond XUV pulses whose bandwidths are naturally broader than 2 eV, such a small sampling interval would lead to large phase errors under the presence of experimental noise, since the spectral phase difference at $\phi^{\mathrm{xuv}}(\omega)$ and $\phi^{\mathrm{xuv}}(\omega-\omega_{21})$ would tend to approach zero as $\omega_{21}$ becomes small. In contrast, as long as the Whittaker-Shannon sampling theorem is satisfied, a larger sampling interval can reduce the ambiguities in determining the spectral phase. As for the maximum energy shear, it is limited by the Whittaker-Shannon sampling theorem. Namely, the energy shear $\hbar\omega_{21}$ should be smaller than the spectral bandwidth of the XUV pulse to be characterized. The minimum energy shear is more complicated. As shown in Eq.(17) of the following section, when the noise contribution exceeds the real spectral phase difference, the reconstruction fails. As a result, the minimum spectral shear depends on the noise fraction and the spectral phase shape of the XUV pulse to be characterized. More detailed comparisons of the present scheme and the Cs-SPIDER will be given in the next section under the presence of experimental noises.

## 3. Error Estimation under Noisy Environments

In order to show the merit of our scheme we will do the error estimation under noisy environments in this section. Since the pulse shape may affect the reconstruction fidelity, we consider three different pulse shapes for the attosecond XUV probe which are shown in Fig. 3, where we plot the temporal intensity and temporal phase. The inset of each graph shows the corresponding spectral intensity and spectral phase. All pulses have a Gaussian spectral shape with a FWHM of 20 eV, corresponding to the transform-limited (TL) pulse duration of 91 as. Their spectral phases can be generally described by a polynomial,

$$\phi^{\mathrm{xuv}}(\omega) = a(\omega-\omega_0^{\mathrm{xuv}})^2 + b(\omega-\omega_0^{\mathrm{xuv}})^3, \tag{16}$$

where $\omega_0^{\mathrm{xuv}}$ is the central frequency of the probe pulse. Specifically we choose $\hbar\omega_0^{\mathrm{xuv}} = 30$ eV based on the recent experimental work at this photon energy [17], and additionally assume a 20 eV spectral bandwidth. Of course our scheme is rather general, and can be applied to any other XUV photon energies. The pulse in Fig. 3(a) corresponding to the case of $a = 0$ and $b = 0$ is transform-limited with a constant phase. The pulse in Fig. 3(b) corresponding to the case of $a = 6\times10^{-3}$ rad/eV$^2$ and $b = 0$ (quadratic spectral phase) is linearly chirped by a factor of two

in terms of pulse duration. Similarly, the pulse in Fig. 3(c) corresponding to the case of $a = 0$, $b = 5 \times 10^{-4}$ rad/eV$^3$ (cubic spectral phase) is quadratically chirped. Now we will reconstruct these three different pulse shapes in the time domain, compare them with the original input pulse shapes, and estimate the error in terms of the temporal intensity and temporal phase under the possible experimental noises.

Since the photoelectron quantum beat given by Eq. (6) is the experimentally measurable quantity in our scheme, reconstruction errors would come from the experimental fluctuations in the photoelectron signals. The fluctuations may be intensity as well as phase fluctuations in the beat signals. The noisy quantum beat signal can be expressed as

$$S^{\mathrm{xuv}}_{\mathrm{noisy}} \propto (\sqrt{I^{\mathrm{xuv}}(\omega) I^{\mathrm{xuv}}(\omega - \omega_{21})} + I_{\mathrm{n}}) \cos\left[\omega_{21}\tau + \phi_c - \Delta\phi^{\mathrm{xuv}}_{\mathrm{noisy}}(\omega)\right] + S_{\mathrm{n}} \tag{17}$$

where $\Delta\phi^{\mathrm{xuv}}_{\mathrm{noisy}}(\omega)$ is the noisy spectral phase difference, $I_{\mathrm{n}}$ is the multiplicative amplitude (intensity) noise, and $S_{\mathrm{n}}$ is the additive amplitude (intensity) noise. $I_{\mathrm{n}}$ and $S_{\mathrm{n}}$ are caused by the fluctuation of the signal intensity which arises from the electronic and thermal noises in the detector, etc. A good thing for the reconstruction scheme from the quantum beat is that the reconstructed result is not very sensitive to the fluctuation of the signal intensity. This is so, since, if we want to extract the spectral phase difference, the quantum beat signal expressed in Eq. (17) needs to be Fourier-transformed to the frequency domain (energy domain) where only the peak at frequency $\omega_{21}$ is selected for the determination of the phase difference, $\Delta\phi^{\mathrm{xuv}}_{\mathrm{noisy}}(\omega)$. During this selecting process, the additive amplitude noise, $S_{\mathrm{n}}$, which serves as a background noise around the peak, can be filtered out. As for the multiplicative amplitude noise, $I_{\mathrm{n}}$, it does not influence the phase offset of the beat signal, although it does influence the beat signal amplitude. In contrast, the phase noise is produced when separate measurements with different delay times, $\tau$, are performed by separate probe shots. Clearly it cannot be easily filtered out in our scheme, and therefore the phase noise is the major source of reconstruction errors.

After these considerations, we add a pseudo-random number to each measured spectral phase difference in order to simulate their effects [20], i.e.,

$$\Delta\phi^{\mathrm{xuv}}_{\mathrm{noisy}}(\omega) = \Delta\phi^{\mathrm{xuv}}_{21}(\omega) + \frac{\alpha}{n}\eta, \tag{18}$$

where $\Delta\phi^{\mathrm{xuv}}_{\mathrm{noisy}}(\omega)$ is the spectral phase difference of the XUV probe pulse to be characterized with a phase fluctuation, $\Delta\phi^{\mathrm{xuv}}_{21}(\omega)$ is the ideal (fluctuation-free) spectral phase difference, $\alpha$ is the noise fraction, and $\eta$ is a pseudo-random number assuming a Poisson distribution of mean value $n$. In this simulation, we set $n = 3.14$ and the noise fraction $\alpha = 0.2$ (20 %). Assuming three different probe pulse shapes introduced in Fig. 3, we carry out the reconstruction procedure described in Sec. 2 using two different amounts of the energy shear, $\Delta E_e = 0.069$ eV and 1.9 eV. The results are shown in Figs. 4(a)-(f) and Figs. 4(g)-(l), respectively. To compare the reconstruction fidelities with these two energy shears quantitatively, we now introduce $\varepsilon_I$ and $\varepsilon_\phi$ to describe the temporal intensity and phase errors, respectively. The temporal intensity error $\varepsilon_I$ is defined by [20]

$$\varepsilon_I = \sqrt{\frac{1}{N}\sum_{j=1}^{N}[I_{\mathrm{input}}(t_j) - I_{\mathrm{noisy}}(t_j)]^2}. \tag{19}$$

where $N$ is the number of elements in the temporal list. The value of $N$ is equivalent to the number of sampling points in the energy domain. In our numerical simulation, $N = 120$ and the spectral range for Fourier transformation is set from 0 eV to 60 eV. $I_{\mathrm{input}}(t_j)$ is the input temporal intensity for the j-th element of the corresponding list to time slot $t_j$, and $I_{\mathrm{noisy}}(t_j)$ is the reconstructed temporal intensity for the j-th element. Since the input pulse has been scaled

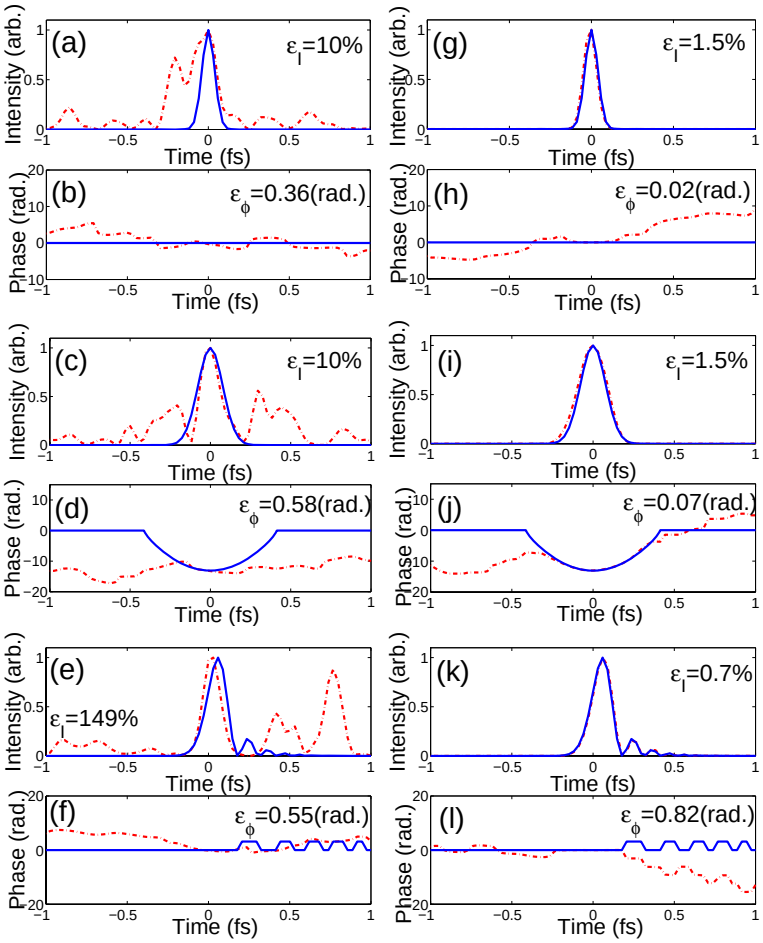


Fig. 4. Comparison of reconstructed probe pulses by noisy beat signals with two different energy shears, (a)-(f) $\Delta E_e = 0.069$ eV and (g)-(l) $\Delta E_e = 1.9$ eV. The solid and dashed lines in each graph correspond to the input pulse and reconstructed pulse under noise with $\alpha = 0.2$. The definitions and the physical meanings of $\varepsilon_I$ and $\varepsilon_\phi$ are given in the text. (a) and (g) Temporal intensity for the transform-limited (TL) pulse input. (b) and (h) Temporal phase for the TL pulse input. (c) and (i) Temporal intensity for the linearly chirped pulse input. (d) and (j) Temporal phase for the linearly chirped pulse input. (e) and (k) Temporal intensity for the quadratically chirped pulse input. (f) and (l) Temporal phase for the quadratically chirped pulse input. The central photon energy and the spectral bandwidth of the probe pulse is $\hbar\omega_0^{\mathrm{xuv}} = 30$ eV and 20 eV, respectively.

to have a unit amplitude, the temporal intensity error $\varepsilon_I$ may be regarded as a percentage error. The definition of the temporal phase error $\varepsilon_\phi$ is [20]

$$\varepsilon_\phi = \frac{\sqrt{\frac{1}{N}\sum_{j=1}^{N} I_{\mathrm{input}}^2(t_j)[\phi_{\mathrm{input}}(t_j) - \phi_{\mathrm{noisy}}(t_j)]^2}}{\sqrt{\frac{1}{N}\sum_{j=1}^{N} I_{\mathrm{input}}^2(t_j)}}, \tag{20}$$

where $\phi_{\mathrm{input}}(t_j)$ is the input temporal phase for the j-th element in the temporal list, and $\phi_{\mathrm{noisy}}(t_j)$ is the reconstructed temporal phase for the j-th element. Note that the phase error has a unit of

radian.

By comparing the results shown in Fig. 4 with the $\Delta E_e = 0.069$ eV and 1.9 eV energy shears, we can see that the use of the large energy shear proposed in our scheme ($\Delta E_e = 1.9$ eV) is a better choice for the more accurate reconstruction of attosecond pulses.

## 4. Effects of the Chirp of the Pump Pulse

For the case of optical SPIDER, what is measured is optical interference between the pulse to be characterized and its frequency-sheared replica. In our case, we measure interference (quantum beat) in the photoelectron spectrum induced by the UV∼VUV pump and attosecond XUV probe pulses as a function of time delay. That is, our scheme as well as the one described in Ref. [15], both of which are the variants of photoelectron SPIDER, require the use of a pump pulse. A natural question is whether and how much the chirp of the pump pulse affects the reconstruction of the attosecond XUV pulse. This question is particularly relevant from the experimental point of view, since a relatively low-order HHG pulse, which are known to be more or less chirped, may be immediately used as a pump pulse. In this section we will show that the chirp of the pump pulse does not at all spoil the reconstruction of the attosecond XUV pulse.

Recall that Eq. (6) has been derived for the pump and probe pulses with an arbitrary temporal shape and spectral phase, and such information for the pump pulse is reflected in the complex probability amplitudes, $C_1$ and $C_2$, and their relative phase, $\phi_c (= \arg[C_1^* C_2])$. By realizing this fact, it is rather obvious, without any analysis, that a chirp of the pump pulse would not affect the determination of the spectral phase, since those terms simply remain constants through the repeated measurements by changing the delay, $\tau$. However, the chirp of the pump pulse does influence the *contrast* of the beat signal, which is also obvious from Eq. (6). We now carry out some analysis to find the relation between the beat contrast and the linear chirp rate of the pump pulse.

Assuming that the pump pulse is linearly chirped, the electric field amplitude of the pump pulse is given by

$$E^{\rm pump}(t) = E_0 \exp\left[-i\omega_0^{\rm pump} t - \frac{t^2}{2\tau_p^2(1-i\xi)}\right], \tag{21}$$

where $E_0$ and $\omega_0^{\rm pump}$ are the peak field amplitude and the central frequency of the pump pulse, respectively, and $\xi$ is a dimensionless chirp parameter where positive (negative) $\xi$ means that the instantaneous frequency increases (decreases) with time. The time duration for the FWHM (full width at half maximum) of the linearly chirped pump pulse is given by $\tau^{\rm pump} = 2\tau_p\sqrt{\ln 2}\sqrt{1+\xi^2}$ with $2\tau_p\sqrt{\ln 2}$ being the pulse duration of the transform-limited pulse with the same spectral width. Note that the peak of the pump pulse always arrives at $t = 0$. As for the atom, we assume that it is initially in the ground state. The time-dependent amplitude equations for the system consisting of $|0\rangle$, $|1\rangle$, and $|2\rangle$ irradiated by the pump pulse read

$$\begin{aligned}
\dot{C}_0(t) &= i\frac{\mu_{01}}{2\hbar}E^{\rm pump}(t)C_1(t)\exp[-i\omega_1 t] + i\frac{\mu_{02}}{2\hbar}E^{\rm pump}(t)C_2(t)\exp[-i\omega_2 t] \\
\dot{C}_1(t) &= i\frac{\mu_{10}}{2\hbar}E^{\rm pump}(t)C_0(t)\exp[i\omega_1 t] \\
\dot{C}_2(t) &= i\frac{\mu_{20}}{2\hbar}E^{\rm pump}(t)C_0(t)\exp[i\omega_2 t],
\end{aligned} \tag{22}$$

where $\omega_k$ $(k = 1,2)$ represents the eigen frequency of state $|k\rangle$, and $\mu_{k0}$ is the bound-bound

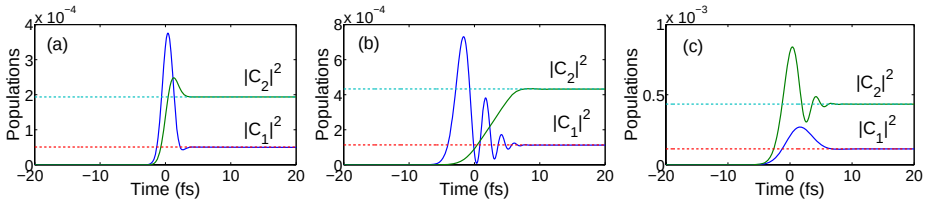


Fig. 5. Population of each excited state as a function of time under the weak pumping condition. The pump pulse is a (a) transform-limited pulse ($\xi = 0$), (b) positively chirped pulse ($\xi = 2$), and (c) negatively chirped pulse ($\xi = -2$). The solid lines (blue for $|C_1|^2$ and green for $|C_2|^2$) are the numerical results obtained by numerically solving the time-dependent Schrödinger equation for H atoms, and the dashed lines (red for $|C_1|^2$ and cyan for $|C_2|^2$) are the analytical results obtained by Eq. (24). The pump pulse parameters employed for all the calculations are, $I_0 = 10^{11}\mathrm{W/cm}^2$ for the peak intensity, $\tau_{\mathrm{TL}}^{\mathrm{pump}} = 2\tau_p\sqrt{\ln 2} = 2$ fs for the transform-limited pulse duration (FWHM), and $\hbar\omega_0^{\mathrm{pump}} = 11.4$ eV for the central photon energy, respectively.

dipole moment between states $|0\rangle$ and $|k\rangle$.

If we assume that the low-order HHG is used for the pump pulse, the peak intensity would be rather modest, say, $10^{11}\mathrm{W/cm}^2$ [17, 21, 22], for which $|C_{1,2}(t)| \ll 1$ and $C_0(t) \sim 1$ for all $t$. Under this weak pumping condition, we can simplify the expressions for the excited states as

$$C_k(t) = i\frac{\mu_{k0}}{2\hbar}\int_{-\infty}^{t} E^{\mathrm{pump}}(t')\exp[i\omega_k t']dt' \quad (k = 1,2). \tag{23}$$

When the pump and probe pulses are well separated in time ($t \gg \tau^{\mathrm{pump}}$), we can analytically solve Eq. (23). Namely, after the pump pulse is over and before the probe pulse arrives, the complex probability amplitude of state $C_k(k = 1,2)$ is obtained to be

$$C_k \simeq i\frac{\mu_{k0}}{2\hbar}\tilde{E}^{\mathrm{pump}}(\omega_k) \quad (k = 1,2), \tag{24}$$

where $\tilde{E}^{\mathrm{pump}}(\omega_k)$ is the electric field amplitude of the pump pulse at frequency $\omega_k$, i.e.,

$$\tilde{E}^{\mathrm{pump}}(\omega_k) = E_0\tau_p\sqrt{1-i\xi}\sqrt{2\pi}\exp\left[-\frac{\tau_p^2(1-i\xi)}{2}(\omega_k - \omega_0^{\mathrm{pump}})^2\right]. \tag{25}$$

In Fig. 5 we plot representative results for the population of each excited state as a function of time by numerically solving the time-dependent Schrödinger equation to compare with the analytical solutions given in Eq. (24). The solid curves in Fig. 5 are associated with the coherent transients [23]. The pump pulse parameters employed for all calculations are, $I_0 = 10^{11}\mathrm{W/cm}^2$ for the peak intensity, $2\tau_p\sqrt{\ln 2} = 2$ fs for the pulse duration (FWHM) of the transform-limited pulse, and $\hbar\omega_0^{\mathrm{pump}} = 11.4$ eV for the central photon energy, respectively. Clearly under the weak pumping condition the analytical solutions for $|C_1|^2$ and $|C_2|^2$ agree well with the numerical solutions. Substitution of Eq. (24) into Eq. (6) leads to the following equation for the beat signal at the magic angle:

$$\begin{aligned} S_{21}(\varepsilon,\Theta_0,\tau) \propto\ & \mathscr{R}_{s1}\mathscr{R}_{s2}\mathscr{R}_{10}\mathscr{R}_{20}\sqrt{I^{\mathrm{pump}}(\omega_1)I^{\mathrm{pump}}(\omega_2)} \\ & \times\sqrt{I^{\mathrm{xuv}}(\omega)I^{\mathrm{xuv}}(\omega-\omega_{21})}\cos\left[\omega_{21}\tau + \phi_c - \Delta\phi_{21}^{\mathrm{xuv}}(\omega)\right], \end{aligned} \tag{26}$$

in which $\mathscr{R}_{k0}$ $(k = 1,2)$ is the radial component of the bound-bound dipole moment between

$|0\rangle$ and $|k\rangle$, and $I^{\rm pump}(\omega_k)$ represents the spectral intensity of the pump pulse at the frequency $\omega_k$ ($k = 1, 2$), i.e.,

$$I^{\rm pump}(\omega_k) = 2\pi E_0^2 \tau_p^2 \sqrt{1+\xi^2} \exp\left[-\tau_p^2(\omega_k - \omega_0^{\rm pump})^2\right]. \tag{27}$$

Using Eq. (24) the phase offset, $\phi_c$, can also be rewritten as

$$\phi_c = \tau_p^2 \xi\, \omega_{21}(\omega_{\rm av} - \omega_0^{\rm pump}), \tag{28}$$

where $\omega_{\rm av} = (\omega_1 + \omega_2)/2$ represents the averaged frequency of the excited states. From Eq. (28) we see that the phase offset, $\phi_c$, becomes zero if there is no chirp ($\xi = 0$) or the photon energy of the pump pulse coincides with the averaged frequency of the excited states. However, as we have briefly mentioned in the beginning of this section, we emphasize that the value of $\phi_c$ itself does not affect the reconstruction process of the spectral phase of the attosecond pulse: Once the excitation by the pump pulse has been completed, $\phi_c$ serves as a constant term in the quantum beat signal [see Eq. (26)]. Since what matters for the reconstructed spectral phase is a *relative* phase distribution in the frequency/energy domain, a constant phase offset would not affect this relative phase distribution. We would like to mention that, although we have carried out the detailed analysis for the pump pulse with a linear chirp, it is clear that the presence of the *nonlinear chirp* in the pump pulse would not affect the determination of the spectral phase distribution of the attosecond pulse, either.

With the aid of simple expressions obtained above, we can now define the *beat contrast* for the case of linearly chirped pump pulse. According to Eq. (26), the ratio of the two-photon ionization probability amplitudes through the bound states $|1\rangle$ and $|2\rangle$ is

$$r_{12} = \frac{\mathscr{R}_{s1}\mathscr{R}_{10}}{\mathscr{R}_{s2}\mathscr{R}_{20}} \exp\left[\tau_p^2 \omega_{21}(\omega_{\rm av} - \omega_0^{\rm pump})\right] \sqrt{\frac{I^{\rm xuv}(\omega)}{I^{\rm xuv}(\omega - \omega_{21})}}. \tag{29}$$

Note that the last coefficient associated with the XUV in Eq. (29) is reduced to unity if $I^{\rm xuv}(\omega) \sim I^{\rm xuv}(\omega - \omega_{21})$. As we expect, the beat contrast turns out to be high if the two ionization probability amplitudes have comparable magnitudes, and naturally it reaches maximum when they are exactly equal. Eq. (29) implies that the beat contrast has nothing to do with the chirp of the pump pulse, but it is related to the central frequency of the pump pulse. That is, if we could adjust the central frequency of the pump pulse, we can obtain the maximum beat contrast which would lead to the better experimental accuracy.

## 5. Effects of the broad bandwidth of the pump pulse

Since we have assumed that the pump pulse has a broad bandwidth so that it can coherently excite two bound states with an energy separation of a fraction of eV to a few eV, more than two states may be coherently excited, depending on the choice of atoms and the bandwidth as well as the central photon energy of the pump pulse. Naively we can argue that the coherent excitation of more than two states would not spoil the reconstruction process for the spectral phase, since it simply brings new beat frequencies in the photoelectron signals when plotted as a function of delay time between the pump and probe pulses, which can be easily removed by applying an appropriate frequency filter. That is indeed the case, and in this section we will show how it actually works through numerical simulations.

Specifically we assume that the central photon energy and the bandwidth of the pump pulse is $\hbar\omega_0^{\rm pump} = 11.4$ eV and $\hbar\Delta\omega^{\rm pump} = 2$ eV (FWHM), respectively. We also assume that the attosecond XUV pulse to be characterized has a central photon energy at $\hbar\omega_0^{\rm xuv} = 30$ eV with a bandwidth of $\hbar\Delta\omega^{\rm xuv} = 6$ eV (FWHM), and $\xi = \sqrt{3}$. As shown in Fig. 1, the $4p$ state labeled

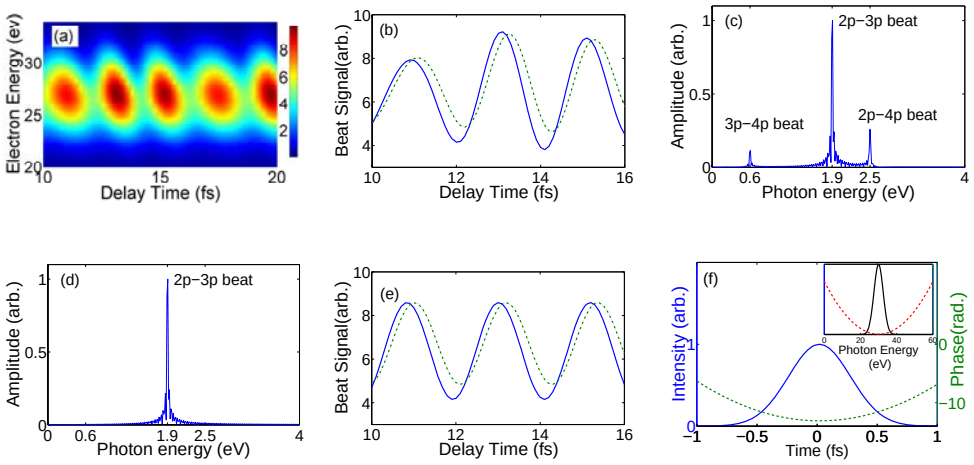


Fig. 6. Reconstruction of the electric field for the case in which the pump pulse coherently excites *three* states instead of two. (a) Numerical simulation of the photoelectron spectra as functions of delay time and electron energy. Note that the signal contains the contribution of three beats, i.e., $2p$-$3p$, $3p$-$4p$, and $2p$-$4p$ beats. (b) Beat signals at the photoelectron energy of $\varepsilon = 28$ eV (blue solid line) and 26 eV (green dashed line). (c) The Fourier transform of the beat signal shown in graph (b) at $\varepsilon = 28$ eV. (d) Applying the frequency filter, only the selected spectral peak for $2p-3p$ is seen. (e) The Inverse-Fourier transform of the selected $2p$-$3p$ peak in the time domain. (f) The reconstructed temporal envelope function (blue solid line) and the temporal phase (green dashed line), with the corresponding spectral intensity (black solid line) and spectral phase (red dashed line) shown in inset.

as $|3\rangle$ are now excited by the spectral wing of the pump pulse. Therefore the coherent superposition prepared by the pump pulse consists of *three* states, $|1\rangle$, $|2\rangle$, and $|3\rangle$, leading to the appearance of the three beat frequencies in the photoelectron spectrum, which we call $3p$-$4p$ and $2p$-$4p$ beats in addition to the $2p$-$3p$ beat. The numerically obtained photoelectron signal at the detection angle of $\Theta_0$ is shown in Fig. 6(a). Fig. 6(b) presents two representative beat signals obtained at two different photoelectron energies, $\varepsilon = 28$ and 26 eV. Clearly these two beat signals exhibit slightly different modulations due to the presence of the three beat frequencies with different weighting factors and phase factors, as one can easily imagine from Eq. (6) for the case of two states. By taking a Fourier transform of Fig. 6(b), we find three peaks in the energy domain, as shown in Fig. 6(c). Since we have set the central photon energy of the pump pulse at $\hbar\omega_0^{\rm pump} = 11.4$ eV, the population probability in $|3\rangle$ is much smaller than those in $|1\rangle$ and $|2\rangle$. Hence the Fourier amplitudes for the $3p-4p$ and $2p-4p$ beats are much smaller than that for the $2p-3p$ beat. By applying an appropriate frequency filter on Fig. 6(c) to select the $2p-3p$ beat only, we obtain Fig. 6(d). After taking an Inverse Fourier transform of Fig. 6(d), we uniquely obtain the beat signals back in the time domain, which are shown in Fig. 6(e). From the phase offsets in these beats we can retrieve the phase differences between every two frequency components of the attosecond XUV pulse, and subsequently reconstruct the spectral phase. The reconstructed spectral field and temporal field are shown in Fig. 6(f). Thus we have demonstrated that our scheme works well even if the broadband pump pulse excites more than two states.

## 6. Applicability for a pulse train and other atoms

So far we have assumed isolated pulses for both pump and probe pulses. Since HHG may be conveniently used as a source for both pump and probe pulses, either or both of them may be in the form of a pulse train(s). It is worthwhile to discuss whether our scheme is applicable for such cases.

First we consider the case of an isolated pulse for the pump and a pulse train for the probe. If the bandwidth of each subpulse to be characterized is sufficiently wider than the sampling interval, $\omega_{21}$, the quantum beat(s) can be seen and the present scheme should work as already discussed in Ref. [15]. However, in some case the bandwidth of each subpulse in the probe pulse train may be relatively narrow. For such a case, we could use a pair of bound states, say, $3p$ and $4p$ ($\Delta E_e = 0.66$ eV) instead of $2p$ and $3p$ ($\Delta E_e = 1.9$ eV), to make the energy shear smaller. Alternatively, the use of an even smaller energy shear, $\Delta E_e = 0.069$ eV, with the Cs-SPIDER [15] may be a good choice.

Now consider the case of a pulse train for the pump and isolated pulse or pulse train for the probe. We would often face this situation if we use low-order harmonics of a Ti:Sapphire laser as a VUV pump pulse, since not-very-selective optics are usually employed to avoid the loss of pulse energy of harmonics. As a result, the VUV pump pulse consists of more than one harmonic order with a photon energy interval of $\sim$3 eV and the associated spectral bandwidth of $\sim$2 eV or less. Recalling the fact that the energy separation between the two beating atomic levels is 1.9 eV in our specific example, it is now clear that, when one harmonic component of the pump pulse is near resonant with the atomic transitions, all other harmonic components are far off-resonant without making any contribution to the beat signal. Therefore our scheme should work even if the pump pulse is a pulse train. We note that, as we have recently shown, interactions of atoms and a pulse train in the weak field (multiphoton ionization) regime can be most easily understood in the frequency domain rather than in the time domain [24]. Another important remark is that the well-defined phase relationship between the neighboring harmonics of the VUV pump pulse is not required unless the energy interval between the neighboring harmonics is so small that more than one harmonic contribute to the pump process. Obviously this is not the case if the VUV pump pulse is provided by the low-order harmonics of a Ti:Sapphire laser.

Before closing this section, we would like to emphasize that, although we have specifically presented our numerical results for the H atom, our scheme should work for other atoms such as He and Cs atoms. Which atom and states we should employ to apply our scheme depends on the photon energy of the VUV pump pulse, and if the VUV pump pulse is provided by the low-order harmonics of a Ti:Sapphire laser, we must a little bit tune the fundamental photon energy. In our case, we have assumed that the 11.4 eV VUV pump pulse is provided by the 7th harmonic of the Ti:Sapphire laser at 761 nm. On the other hand, if we choose 2p and 3p states of He, we could produce the 22.5 eV VUV pump pulse by the 15th harmonic of a Ti:Sapphire laser at 826 nm. Similarly, if we choose 7p and 8p states of Cs, the second harmonic of a Ti:Sapphire laser at $\sim$800 nm can be conveniently used for the UV pump pulse. Of course the energy shear we can obtain by using 7p and 8p of Cs is smaller. But it is still 25 times larger than the case of a Cs fine structure doublet, and we receive benefit from the large energy shear to improve the fidelity of attosecond pulse reconstruction.

## 7. Conclusions

In conclusion, we have presented a new variant of photoelectron SPIDER which is suitable to characterize attosecond XUV pulses. A UV$\sim$VUV pulse from the low-order HHG may be conveniently used as a pump pulse to coherently excite two bound states with an energy separation of a fraction of eV to a few eV, which serves as a energy shear in the photoelectron signal. The

most important property of our scheme is its capability to characterize attosecond XUV pulses down to a few hundred attoseconds or even less with a sufficient accuracy. The reconstruction algorithm is very similar to that of the optical SPIDER, which is simple and robust against noise.

We have quantitatively examined the capability and also the limitation of the present scheme from a few different aspects. Perhaps most importantly we have shown that the chirp of the pump pulse does not spoil the reconstruction of the attosecond pulse, and the beat contrast in the photoelectron spectrum can be maximized by adjusting the central photon energy for the pump pulse. We have also studied the influence of the finite width for the detection angle of photoelectrons. It is interesting to point out that, although the detection angle should be ideally at the magic angle with an infinitely small angle width, a rather large detection angle (as much as $\pm\ 20^{o}$) only introduces the spectral phase errors of about $1^{o}$ in the spectral phase distribution for the XUV probe photon energy up to $\sim$60 eV for the case of H atom. We have also found that, although the broad bandwidth of the pump pulse may excite more than two bound states, undesired frequency components in the beat signal can be easily filtered out in the frequency domain and hence does not spoil the reconstruction of the attosecond pulse. We hope that our scheme will serve as an alternative method to characterize attosecond XUV pulses.

**Acknowledgement**

This work was supported by a Grant-in-Aid for scientific research from the Ministry of Education and Science of Japan.